

On the Formation and Properties of Fluid Shocks and Collisionless Shock Waves in Astrophysical Plasmas

A. Bret^{1,2} and A. Pe'er³

¹*ETSI Industriales, Universidad de Castilla-La Mancha, 13071 Ciudad Real, Spain*

²*Instituto de Investigaciones Energéticas y Aplicaciones Industriales, Campus Universitario de Ciudad Real, 13071 Ciudad Real, Spain.*

³*Department of Physics, University College Cork, Cork, Ireland*

(Dated: December 3, 2024)

Abstract

When two plasmas collide, their interaction can be mediated by collisionless plasma instabilities or binary collisions between particles of each shell. By comparing the maximum growth rate of the collisionless instabilities with the collision frequency between particles of the shells, we determine the critical density separating the collisionless formation from the collisional formation of the resulting shock waves. This critical density is also the density beyond which the shock downstream is field free, as plasma instabilities do not have time to develop electromagnetic patterns. We further determine the conditions on the shells initial density and velocity for the downstream to be collisional. If these quantities fulfill the determined conditions, the collisionality of the downstream also prevents the shock from accelerating particles or generating strong magnetic fields. We compare the speed of sound with the relative speed of collision between the two shells, thus determining the portion of the parameters space where shock formation is possible for both classical and degenerate plasmas. Finally, we discuss the observational consequences in several astrophysical settings.

I. INTRODUCTION

Shock waves are among the most ubiquitous and most studied physical phenomena. They exist in many different astronomical objects, on very many different scales. They play a major role in shaping the observed signal of various objects, providing (1) a natural way of depositing kinetic energy; (2) the necessary conditions for acceleration of particles to high energies, non-thermal distribution; and furthermore, (3) shock waves may be responsible for generating strong magnetic fields [1–4].

Shock waves may come in two flavors. In a neutral fluid, kinetic energy dissipation at the shock front is provided by binary collisions [58]. As a result, the shock front is a few mean-free-paths thick [5], and the shock is “collisional”. In charged plasma, on the other hand, instabilities prompted by collective behavior can equally mediate shock waves and provide the kinetic energy dissipation at the front [6, 7]. In this case, the shock front can be several orders of magnitudes shorter than the mean-free-path for binary collisions [8]. These shocks have been dubbed “collisionless shocks”.

While there were still doubts about the very existence of collisionless shocks in the late 1980’s [9], in-situ observations of the earth bow-shock, for example, have definitely cast them out [10, 11]. Because they are collisionless, these shocks are formed through collective plasma instabilities, on the time scale of these instabilities [12, 13].

The absence of close collisions allows particles to gain energy without sharing it with others. As a result, collisionless shocks are excellent particle accelerators [14, 15], as opposed to collisional shocks [e.g., 16].

In view of the properties which derive from the absence of collisions, one can wonder about the conditions required for collisionless-ness to be fulfilled. The goal of this paper is to investigate 1/ the conditions required for the shock formation to be collisionless, and 2/ the conditions required for the downstream region to be so.

Regarding the first item, the nature of the shock formation determines the time scale on which it forms. In the collisionless regime, the two colliding shells start passing through each other. The overlapping region quickly turns unstable, generating a turbulence which blocks the flow and triggers the shock formation [12, 13]. Binary collisions between the particles of each shell can be neglected if the (average) collision frequency ν_{ss} is much smaller than the growth-rate δ of the fastest counter-streaming instability involved in the overlapping region.

On the other hand, if $\delta \ll \nu_{ss}$, binary collisions govern the dynamics of the shells encounter. We thus find that a quantitative investigation of the interface between the collisional and the collisionless regimes, comes down to comparing δ and ν_{ss} . Note that such an endeavor only makes sense in a plasma, for in a non-ionized collisionless medium, counter-streaming flows are stable ($\delta = 0$) and can only be disrupted by binary collisions.

Still for the first item, the nature of the shock formation determines the electromagnetic patterns that will be found in the downstream, once the shock is formed. Such patterns, like Weibel filaments [17, 18], are the fruit of plasma instabilities in the collisionless case. If the shock is formed through close binary collisions, these instabilities will not grow and will not be able to seed electromagnetic patterns in the downstream. In turn, the absence of fields in the downstream means the absence of scattering agents for the particles, inhibiting their acceleration.

Regarding the second shock item investigated in this paper, namely, the collisionality of the downstream, it also determines whether or not the shock, once formed, is capable of accelerating particles. The reason for this comes from the fact that particle acceleration in a Fermi process results from back-and-forth motions around the shock front [19]. This is only possible if both the upstream and the downstream are collisionless, so that particles can nearly freely travel between each region, without exchanging energy with the others. But if the downstream happens to be collisional, particles will be trapped inside as soon as they enter it. They will remain embedded into the downstream flow, constantly exchanging energy with the others, and unable to keep it or to close any Fermi acceleration cycle.

This paper is structured as follows. We begin by considering pair plasmas in Section II. In Section II A we calculate the collision frequency ν_{ss} for close Coulomb collisions between particles of the two pair shells. We then compute in Section II B the growth-rate δ of the fastest growing collisionless mode. In Section II C, ν_{ss} and δ are compared, allowing us to determine the portions of the phase space (γ_0, n_0) (initial Lorentz factor and density of the colliding plasma shells) where the shock formation is mediated by collisionless plasmas effects, or inter-shells binary collisions. Finally, Section II D derives the requirements on (γ_0, n_0) for the downstream of the shock, once formed, to be collisional.

We then turn to electron/proton plasmas in section III. We conduct similar calculations as for the pair plasmas case, emphasizing the qualitative difference that results from the difference in instability growth rate in this scenario. Following these theoretical derivations,

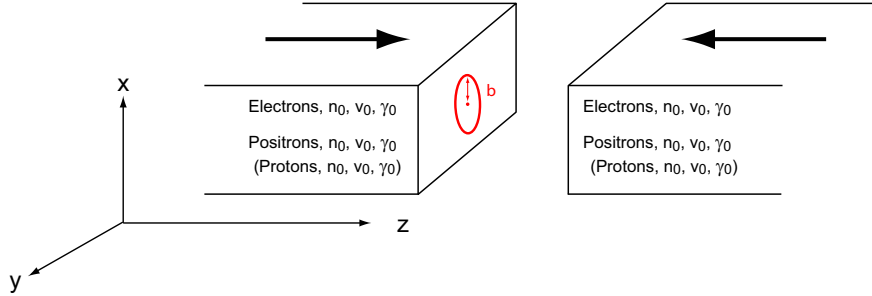


FIG. 1: System considered: two counter-streaming plasmas collide. They are initially cold and symmetric, with electronic density n_0 in the laboratory frame. The first part of the article deals with pair plasmas, while the second part deals with electron/proton plasmas.

we explore the limits of the small velocity spread approximation within each shell used throughout this work in section IV. By equating the speed of sound in the different regimes: classical and quantal gas, Newtonian and highly relativistic, to the speed of collision between the shells, we constrain the parameter space region in which shocks can possibly form. Finally, we discuss in section V the conditions that exist inside several astronomical objects, and the applicability of the theory to these various objects, before we reach our conclusions in section VI.

II. COLLIDING PAIR PLASMA SHELLS

We begin by considering the scenario of two symmetric plasma shells composed of electron-positron pairs heading toward each other, as pictured in Figure 1. Each shell is initially cold (see discussion in Section IV), with initial (lab frame) density n_0 and Lorentz factor $\gamma_0 = (1 - \beta_0^2)^{-1/2}$, where $\beta_0 = v_0/c$ is the normalized flow velocity.

A. Inter-shell collision frequency

The impact parameter for close binary Coulomb collisions is defined via (see Equation (13.4) in [20], with deviation $\theta = \pi/2$)

$$b_C = \frac{q^2}{\gamma_r m_e v_r^2}, \quad (1)$$

where γ_r is the relative Lorentz factor of the two shells, namely $\gamma_r = 2\gamma_0^2 - 1$. The relative velocity of the two shells is

$$v_r = \frac{2\beta_0}{1 + \beta_0^2}c, \quad (2)$$

where clearly $\gamma_r = (1 - v_r^2/c^2)^{-1/2}$. When b_C becomes too small, it has to be replaced by the relevant de Broglie length (see Equation (5.10) in [21]),

$$b_Q = \frac{\hbar}{p} = \frac{\hbar}{\gamma_r m_e v_r}. \quad (3)$$

The frequency for close collisions between particles of two different shells then reads,

$$\nu_{ss} = n_0 v_r \pi b^2 = n_0 \frac{2\beta_0}{1 + \beta_0^2} c \pi \max(b_C, b_Q)^2. \quad (4)$$

Since b_C is proportional to v_r^{-2} and $b_Q \propto v_r^{-1}$, the impact parameter is classical at low velocity, and quantum at high velocity. The two values of the impact parameters become equal at

$$\frac{q^2}{\gamma_r m_e v_{r,eq}^2} = \frac{\hbar}{\gamma_r m_e v_{r,eq}} \Rightarrow \frac{v_{r,eq}}{c} \equiv \beta_{r,eq} = \frac{q^2}{\hbar c} = \alpha, \quad (5)$$

namely at sub-relativistic velocities. Here $\alpha \sim 1/137$ is the fine structure constant.

In terms of β_0 and γ_0 , equality is achieved for

$$\begin{aligned} \gamma_{0,eq} &\equiv \gamma_0^* = \sqrt{\frac{\gamma_{r,eq} + 1}{2}} \sim 1.0000067, \\ \beta_{0,eq} &\equiv \beta_0^* = \sqrt{1 - 1/\gamma_0^{*2}} \sim 0.00365. \end{aligned} \quad (6)$$

We thus find that for $\beta_0 < \beta_0^*$, the frequency of close inter-shells collisions is given by Equation (4) with $\max(b_C, b_Q) = b_C$. For $\beta_0 > \beta_0^*$, it is given by Equation (4) with $\max(b_C, b_Q) = b_Q$.

B. Maximum instability growth-rate δ

In collisionless plasmas, shock formation is triggered by the counter-streaming instabilities that arise when the shells start overlapping. These instabilities are numerous and can be found for wave vectors aligned, normal, or even oblique to the flow [22, 23]. For the present case, the growth-rate of the fastest growing mode is only a function of the Lorentz factor. It has already been determined for any γ_0 in Reference [23]; for completeness, we here recall the main results. Noteworthily, the forthcoming growth-rates are analytically exact.

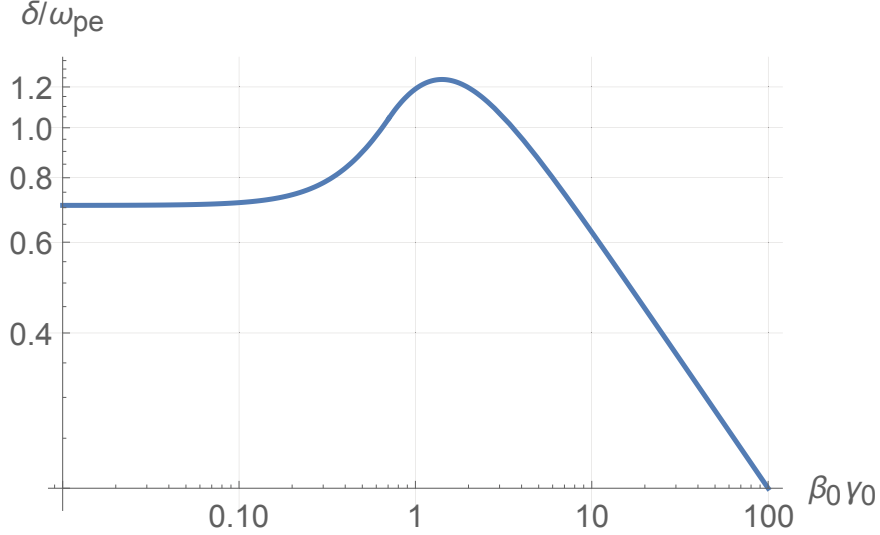


FIG. 2: Growth-rate of the fastest growing mode in terms of $\beta_0\gamma_0$ for cold pair plasmas interaction.

For $\gamma_0 > \sqrt{3/2}$ ($\beta_0 > 1/\sqrt{3}$), the fastest growing mode is the Weibel mode [12], with $\mathbf{k} \perp \mathbf{v}_0$. Its growth-rate is

$$\delta = 2 \frac{\beta_0}{\sqrt{\gamma_0}} \omega_{pe}, \quad (7)$$

where $\omega_{pe} = \sqrt{4\pi n_0 q^2 / m_e}$ is the (electron) plasma frequency. In the opposite regime $\gamma_0 < \sqrt{3/2}$, the fastest growing mode is oblique, with growth-rate

$$\delta = (1 + \beta_0^2) \sqrt{\frac{\gamma_0}{2}} \omega_{pe}. \quad (8)$$

Expressions (7) and (8) are plotted together as functions of $\beta_0\gamma_0$ in Figure 2. The threshold $\gamma_0 = \sqrt{3/2}$ corresponds to $\beta_0\gamma_0 = 1/\sqrt{2}$. The growth rate δ obtains a maximum value $\delta/\omega_{pe} = 2^{3/2}/3^{3/4} = 1.24$ for $\gamma_0 = \sqrt{3}$ ($\beta_0\gamma_0 = \sqrt{2}$).

The existence of a maximum value for the growth-rate δ can intuitively be understood as follows. For plasmas having Lorentz factor $\gamma_0 = \sqrt{3}$ the dominant instability is the Weibel instability (since $\sqrt{3} > \sqrt{3/2}$). This instability is driven by the repulsion of opposite currents [24]. It relies therefore on the Lorentz force being $\propto v_0$. As a result, it weakens at low velocities. Furthermore, this instability weakens at high velocities as well, since v_0 cannot surpass c while the relativistic inertia keeps increasing with γ_0 . These two features are reflected in the scaling of the growth-rate (7), which varies like $\beta_0/\sqrt{\gamma_0}$. With a null limit both at high and low velocities, an intermediate extremum is necessary. Solving $\partial\delta/\partial\gamma_0 = 0$ gives $\gamma_0 = \sqrt{3}$.

C. Comparison of collision rate ν_{ss} and instability growth rate δ

In order to determine whether the shock formed is collisional or collisionless, one needs to compare the frequency for close Coulomb collisions with the fastest growth-rate given above. One singles out three intervals:

1. For $\beta_0 < \beta_0^*$, the impact parameter is classical. The relevant growth-rate in this regime is given by Equation (8). In this scenario, one compares Equation (4) with $b_C > b_Q$ and Equation (8). The calculation gives

$$\frac{\nu_{ss}}{\delta} = \sqrt{\frac{\pi}{128}} \sqrt{\frac{n_0}{N^*}} \frac{1}{\beta_0^3 \gamma_0^{9/2}} \simeq \sqrt{\frac{\pi}{128}} \sqrt{\frac{n_0}{N^*}} \frac{1}{\beta_0^3}. \quad (9)$$

Here,

$$N^* \equiv \left(\frac{mc^2}{q^2} \right)^3 = 4.5 \times 10^{37} \text{ cm}^{-3}. \quad (10)$$

2. For $\beta_0 > \beta_0^*$ and $\gamma_0 < \sqrt{3/2}$, the impact parameter is quantum, while the relevant growth-rate is still given by Equation (8). Comparing Equation (4) but now with $b_C < b_Q$ and Equation (8) gives

$$\frac{\nu_{ss}}{\delta} = \sqrt{\frac{\pi}{8}} \sqrt{\frac{n_0}{N_1^*}} \frac{1}{\gamma_0^{9/2} \beta_0 (1 + \beta_0^2)^2} \simeq \sqrt{\frac{\pi}{8}} \sqrt{\frac{n_0}{N_1^*}} \frac{1}{\beta_0}. \quad (11)$$

Here,

$$N_1^* = \frac{mc^2}{q^2} a_0^{-2} = 1.26 \times 10^{29} \text{ cm}^{-3}, \quad (12)$$

and $a_0 = \hbar^2/mq^2$ is the Bohr radius.

3. For $\gamma_0 > \sqrt{3/2}$, the impact parameter is quantum, while the relevant growth-rate in this case is given by Equation (7). Comparing Equation (4) with $b_C < b_Q$ and Equation 7 gives

$$\frac{\nu_{ss}}{\delta} = \frac{\sqrt{\pi}}{8} \sqrt{\frac{n_0}{N_1^*}} \frac{1}{\gamma_0^{7/2} \beta_0^2 (1 + \beta_0^2)} \simeq \frac{\sqrt{\pi}}{16} \sqrt{\frac{n_0}{N_1^*}} \frac{1}{\gamma_0^{7/2}}. \quad (13)$$

One thus concludes that in all 3 cases, the ratio ν_{ss}/δ has the form

$$\frac{\nu_{ss}}{\delta} = F \times \sqrt{\frac{n_0}{N_i^*}}, \quad (14)$$

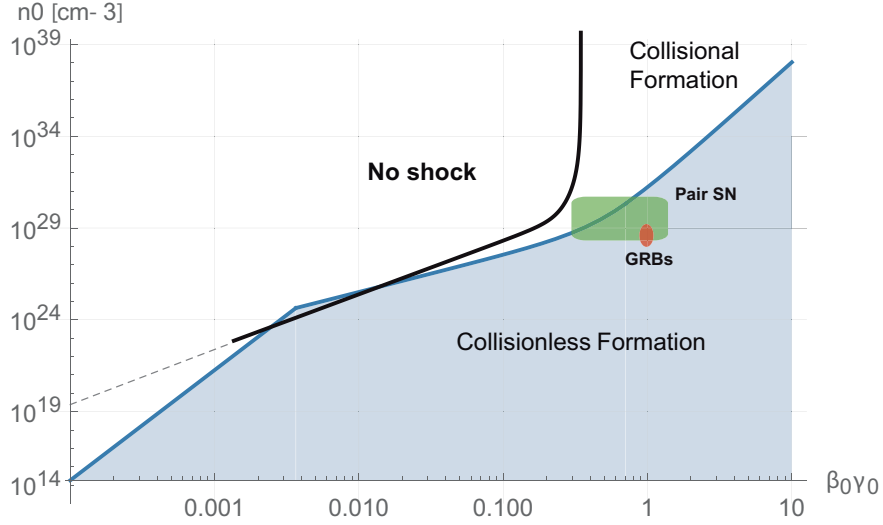


FIG. 3: Critical density beyond which the interaction is collisional for pair plasmas. The blue shaded area of the phase space pertains to collisionless interactions. The colored regions pertain to astrophysical scenarios discussed in Section V. The bold black line pictures the no-shock condition discussed in section IV. As discussed in that section, for $T < T_F$ (the Fermi temperature) shock cannot be formed above this line, for the speed of sound is larger than the collision speed.

where $N_i^* = N^*$ or N_1^* , depending on the scenario considered. The value of the function $F = F(\beta_0)$ is defined through Equations (9, 11, 13), and depends on the scenario considered. We thus conclude that the shock is collisional if

$$\frac{\nu_{ss}}{\delta} > 1 \Rightarrow n_0 > \frac{N_i^*}{F^2}. \quad (15)$$

Figure 3 pictures the critical density beyond which the interaction is collisional. The lower part of the (γ_0, n_0) phase space pertains to collisionless interactions.

D. Conditions on n_0 and γ_0 for a collisionless downstream

After the two shells collide, a shock is formed with a downstream having density n and temperature T . Depending on n and T , the downstream region can be collisionless or collisional - even if initially the shock is formed collisionlessly.

A collisionless plasma is weakly coupled. Indeed, by definition, in a weakly coupled plasma the kinetic energy of the plasma's particles is much larger than the potential energy

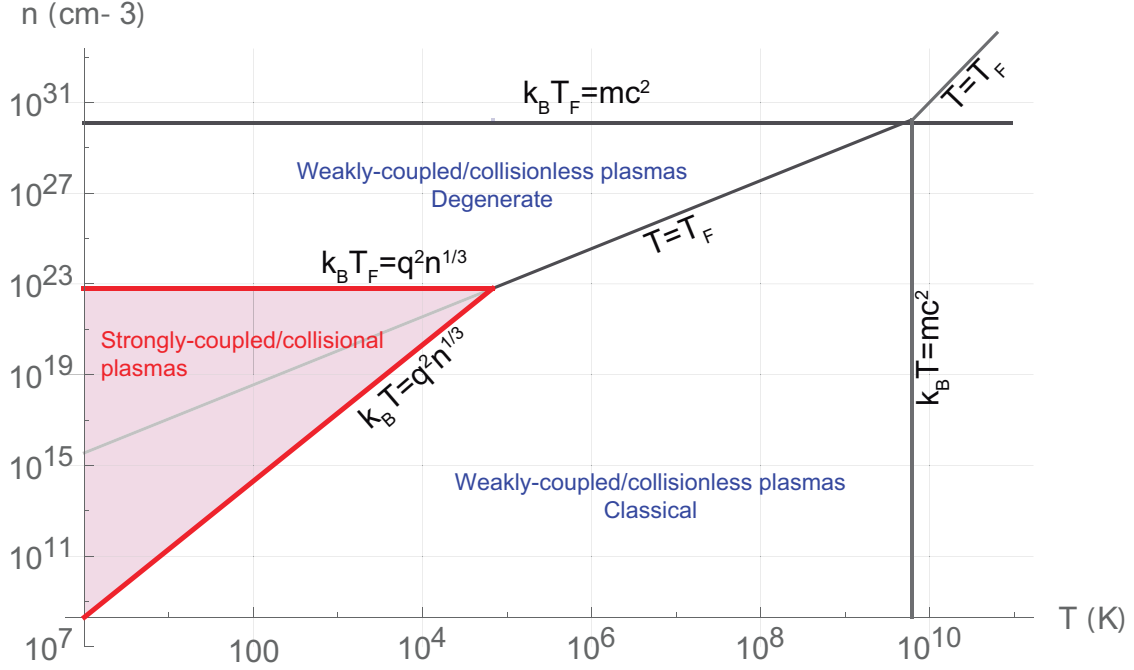


FIG. 4: Collisionless region in the (T, n) phase space. The red shaded area pertains to strongly coupled plasmas, i.e., collisional plasmas. A classical plasma becomes relativistic for $k_B T > mc^2$, and a degenerate plasma becomes relativistic for $k_B T_F > mc^2$.

associated with Coulomb collisions. This, in turn, implies that close Coulomb collisions are rare. The parallel extends even to the degenerate regime, as, for example, the Fermi energy of a weakly coupled degenerate plasma can be found assuming free wave functions (plane waves $\propto e^{i\mathbf{k}\cdot\mathbf{r}}$) for the particles [25].

Figure 4 shows the different plasma regimes in the downstream region, in terms of its temperature and density (T, n) . The line $T = T_F$ pictures plasmas with temperature equals the Fermi temperature. Below this line, $T > T_F$ and the plasma is classical. It is therefore weakly coupled if its kinetic energy is greater than the Coulomb potential, i.e., $k_B T > q^2 n^{1/3}$ [59]. Above this line, $T < T_F$ and the plasma is degenerate. It is therefore weakly coupled if the Fermi energy is greater than the Coulomb potential, $k_B T_F > q^2 n^{1/3}$ [26]. As the Fermi temperature T_F only depends on the density, this latter condition defines a critical density

threshold,

$$\begin{aligned}
k_B T_F &= (3\pi^2 n)^{2/3} \frac{\hbar^2}{2m_e} = q^2 n^{1/3} \\
\Rightarrow n &> \frac{8}{9\pi^4} \left(\frac{m_e q^2}{\hbar^2} \right)^3 = 6.3 \times 10^{22} \text{ cm}^{-3},
\end{aligned}
\tag{16}$$

instead of an oblique line. As a result, plasmas located inside the red triangle pictured in Figure 4 are strongly coupled, i.e., collisional. If the downstream lies in this domain, the shock cannot accelerate particles. Note that at higher densities, the plasma remains collisionless, somewhat counter-intuitively, as it is kept degenerate as the densities increase, until reaching the relativistic limit. Thus, the rest of the phase parameter space is weakly coupled, whether for classical or quantum reasons.

One can notice that the collisional regime has an upper bound, both in temperature and density. For $T > 10^5$ K, or $n > 6.3 \times 10^{22} \text{ cm}^{-3}$, the plasma cannot be collisional. Rather, it must be collisionless.

Given that both n and T are functions of the initial density and Lorentz factors n_0 and γ_0 , one can determine the requirements on the initial plasma parameters (n_0, γ_0) that result in collisional downstream region. From the discussion above, it follows that there are two requirements: (i) for classical plasma regime, it is $k_B T \geq q^2 n^{1/3}$; (ii) for the quantum border of the collisional regime, one requires that the plasma density is $n > 6.3 \times 10^{22} \text{ cm}^{-3}$. We therefore explore the conditions on $n(n_0, \gamma_0)$ and $T(n_0, \gamma_0)$ that fulfill these requirements.

1. Conditions for the downstream to be collisional

We derive in Appendix A the dependence of the downstream density and temperature (n, T) on the initial density and the Lorentz factor, (n_0, γ_0) in the non-relativistic regime, which is the relevant regime here. The relations derived in Equation (A7) enable to derive the conditions for the downstream plasma to be collisional. For quantum plasma, the boundary $n = 6.3 \times 10^{22} \text{ cm}^{-3}$ is equivalent to

$$n_0 = 6.3 \times 10^{22} \left(\frac{\hat{\gamma} - 1}{\hat{\gamma} + 1} \right) \text{ cm}^{-3},
\tag{17}$$

where $\hat{\gamma}$ is the adiabatic index. If the temperature in the downstream is low, $T < T_F$, the plasma in the downstream region is degenerate for initial density n_0 larger than this value.

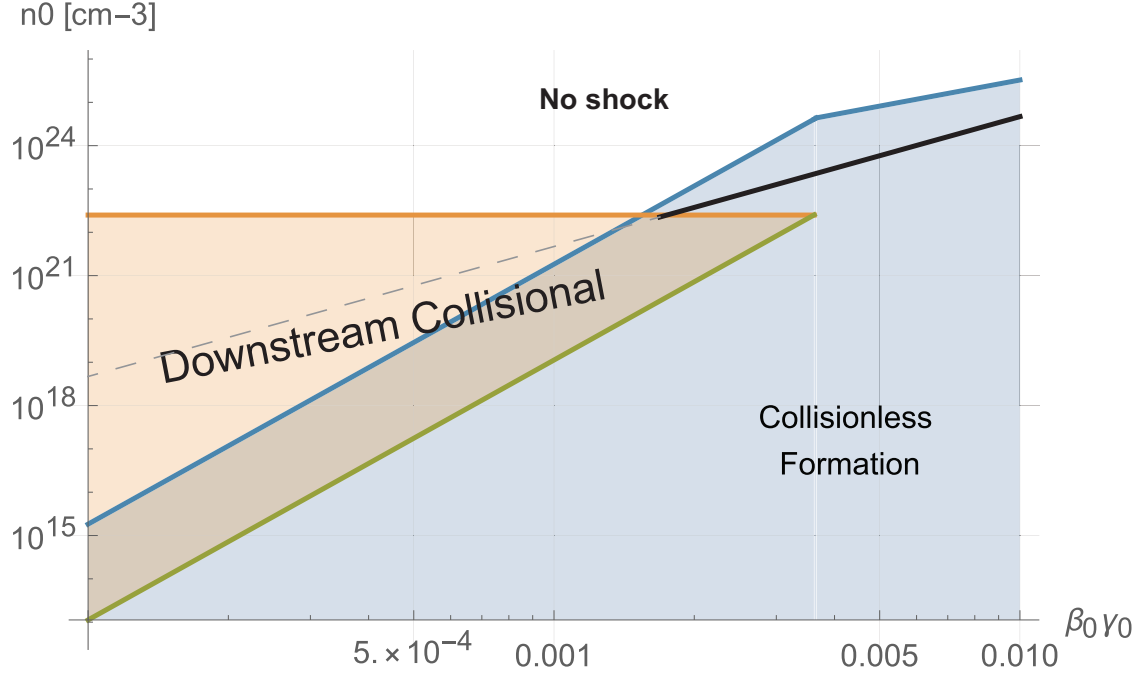


FIG. 5: If the pair plasmas shells have their initial momenta and densities $(\beta_0\gamma_0, n_0)$ located inside the pale orange triangle, the downstream is collisional and the resulting shock cannot accelerate particles. In producing this plot, we consider $\hat{\gamma} = 5/3$. The bold black line pictures the no-shock condition at $T = 0$ discussed in section IV. At $T < T_F$, no shock forms above this line, for the speed of sound becomes larger than the collision speed.

For classical plasma, the boundary is determined by the condition $k_B T = q^2 n^{1/3}$ (see Equation 16). Using Equation (A7), this relation can be written as (γ_0, n_0)

$$\begin{aligned}
 m_e v_0^2 &= q^2 \left(n_0 \frac{\hat{\gamma} + 1}{\hat{\gamma} - 1} \right)^{1/3} \\
 \Rightarrow n_0 &= N^* \left(\frac{\hat{\gamma} - 1}{\hat{\gamma} + 1} \right) \beta_0^6,
 \end{aligned} \tag{18}$$

where $N^* = 4.5 \times 10^{37} \text{ cm}^{-3}$ has been defined in Equation (10). The conditions set in Equations (17, 18) are equal at

$$\beta_0 = \left(\frac{8}{9\pi^4} \right)^{1/6} \alpha = 0.0033 \ll 1, \tag{19}$$

justifying the non-relativistic treatment.

The boundaries defined by Equations (17, 18) are shown in Figure 5, together with the criteria for collisional or collisionless shock formation. If the initial shells are located inside

the pale orange triangle, the downstream of the resulting shock is collisional (fluid); outside of this regime, it is collisionless.

Noteworthily, there is a region of the phase space in which the shock formation is mediated by collisionless instabilities, while the resulting shock has its downstream collisional. This region is enclosed between the blue and the green lines in Figure 5. Comparing Equations (15), (9) and (18), one sees that these two lines are almost exactly parallel, and are separated by a factor

$$\frac{\text{Blue frontier}}{\text{Green frontier}} \sim \frac{128 \hat{\gamma} + 1}{\pi \hat{\gamma} - 1} = 163 \quad \text{for } \hat{\gamma} = 5/3. \quad (20)$$

The upper bounds of the weakly coupled domain displayed on Figure 4 translate to upper-bounds on Figure 5. If the colliding shells have initially either $\beta_0 > 0.0033$ ($v_0 > 1003$ km/s) or $n_0 > 1.57 \times 10^{22}$ cm⁻³ (for $\hat{\gamma} = 5/3$), then the downstream region of the resulting shock is always collisionless. In both cases, particle acceleration can occur.

III. ELECTRON/PROTON PLASMAS ENCOUNTERS

We now adapt the previous results for the case of proton/electron plasmas. The overall dynamic of the system in this scenario is determined by the interaction of the protons. Following the structure of the preceding sections, we first assess the binary collision frequency before turning to the maximum growth-rate.

A. Inter-shells collision frequency

The classical impact parameter for close binary Coulomb collisions in electron-proton plasma reads $b_C = q^2/(\gamma_r m_p v_r^2)$, where m_p is the proton mass (see Equation 1). The quantum impact parameter in this scenario is $b_Q = \hbar/p = \hbar/(\gamma_r v_r m_p)$ (see Equation 3). The close collision frequency between protons of two different shells is therefore

$$\nu_{ss} = n_0 v_r \pi b^2 = n_0 \frac{2\beta_0}{1 + \beta_0^2} c \pi \max(b_C, b_Q)^2. \quad (21)$$

One thus finds that in this scenario as well, the equality $b_C = b_Q$ is reached for $\beta_r = \alpha \sim 1/137$.

B. Growth-rate for the collisionless interaction

In the collisionless regime, the counter-streaming electrons first turn unstable as the shells start overlapping. Once the electronic instability has saturated, the counter-streaming protons turn unstable [27]. In the relativistic regime, the most unstable mode of the counter-streaming protons over the bath of electrons is still the Weibel instability, with a maximum growth-rate given by [28]

$$\delta = 2 \frac{\beta_0}{\sqrt{\gamma_0}} \omega_{pp}. \quad (22)$$

This result is identical to that in Equation (7), after replacing the electron plasma frequency ω_{pe} by the proton plasma frequency $\omega_{pp}^2 = 4\pi n_0 q^2 / m_p$.

In the non-relativistic regime, the same pattern occurs. Electrons are stopped first before the counter-streaming protons become unstable over the bath of electrons. In the limit of small velocity, $\beta_0 \ll 1$, the temperature of this electron bath approaches zero since its thermal energy originates from the initial kinetic energy of the electron beams. The fastest growing mode is found with a \mathbf{k} aligned with the flow [23]. The dispersion equation for the interaction is derived in Appendix B and reads,

$$\frac{2}{x^2} + \frac{R}{(Z-x)^2} + \frac{R}{(x+Z)^2} = 1, \quad (23)$$

where $x = \omega / \omega_{pe}$, $Z = kv_0 / \omega_{pe}$ and $R = m_e / m_p$ is the mass ratio (note that the frequency is measured in units of the *electron* plasma frequency). This equation is solved in Appendix B, yielding the maximum growth-rate for this regime,

$$\delta \sim \frac{\sqrt{3}}{2^{7/6}} R^{1/3} \omega_{pe} = \frac{\sqrt{3}}{2^{7/6}} R^{-1/6} \omega_{pp}. \quad (24)$$

In both the relativistic (Equation 22) and non-relativistic (Equations 24) regimes, the growth rate δ is linear in ω_{pp} , namely it admits the form $\delta = X\omega_{pp}$. In order to fill the gap between these regimes, we have implemented a simple first-order interpolation scheme. We point out that a more accurate fluid model attributing to the electron bath a temperature $3k_B T \sim (\gamma_0 - 1)mc^2$ gives very similar results. Nevertheless, we dim the presentation of the fluid model unnecessary because of (1) its length, (2) the small amount of additional precision it brings, (3) the secondary relevance of this point with respect to the main theme of this work and (4), the fact that the regime corresponding to this interpolation ($\beta_0\gamma_0 \sim 1$) pertains to densities larger than 10^{40} cm^{-3} (see Figure 7).

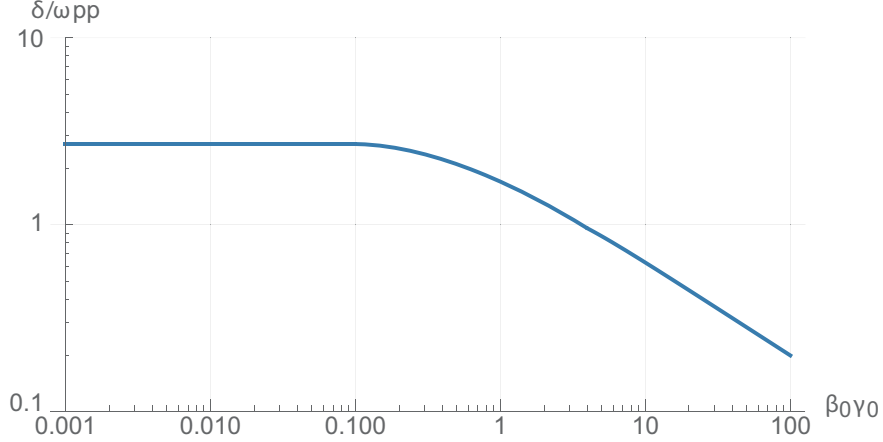


FIG. 6: Growth-rate of the fastest growing unstable mode in terms of $\beta_0\gamma_0$ for electron/proton plasmas interaction. In producing this plot, we took the mass ratio is $R = m_e/m_p = 1/1836$. We interpolated between the non-relativistic (Equation 24) and the relativistic (Equation 22) regimes.

The results of the growth rate are presented in Figure 6. When comparing to the growth-rate for pair plasma in Figure 2, we find that the local extremum has been lost. This feature comes from the main difference between the two settings, namely that for the electron/proton plasma, the proton Weibel instability grows over a bath of electrons.

C. Comparing the collision rate ν_{ss} and the instability growth rate δ

We continue with the road-map of the first part, comparing the time scales for collisional and collisionless interactions in the electron/proton case. In this scenario, we identify four separate regimes.

- For $\beta_r < \alpha = 1/137$, Equation (21) with $\max(b_C, b_Q) = b_C$ is compared with Equation (24). One obtains

$$\frac{\nu_{ss}}{\delta} \sim \frac{\sqrt{\pi/3}}{4 \cdot 2^{5/6}} \sqrt{\frac{n_0}{N^*}} R^{5/3} \frac{(1 + \beta_0^2)^3}{\beta_0^3(2\gamma_0^2 - 1)^2}, \quad (25)$$

where N^* has been defined in Equation (10).

- For $\beta_r > \alpha = 1/137$, yet β_0 still non relativistic, Equation (21) with $\max(b_C, b_Q) = b_Q$, is to be compared with Equation (24). One obtains,

$$\frac{\nu_{ss}}{\delta} \sim 2^{-5/6} \sqrt{\frac{\pi}{3}} \sqrt{\frac{n_0}{N_1^*}} R^{5/3} \frac{(1 + \beta_0^2)}{\beta_0(2\gamma_0^2 - 1)^2} \quad (26)$$

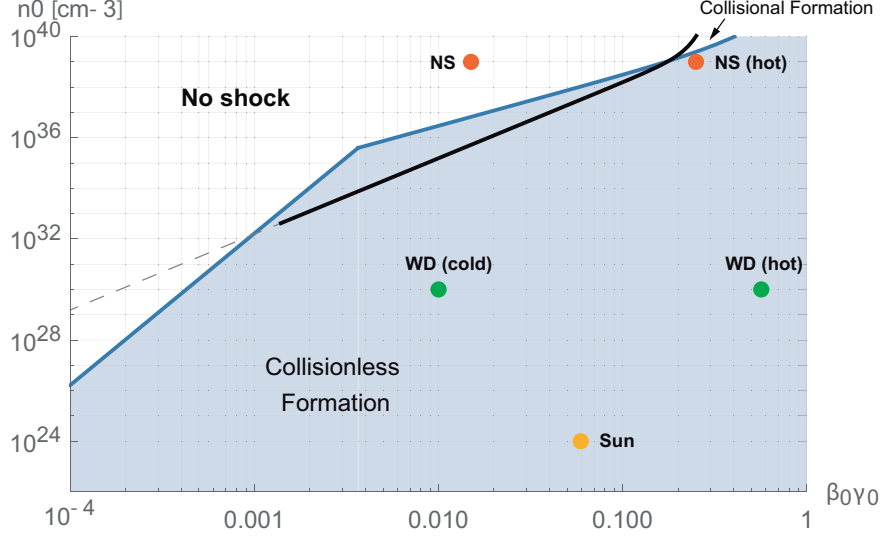


FIG. 7: Frontier between the collisional and the collisionless domains for shock formation in the case of electron/proton plasmas. The colored regions pertain to astrophysical scenarios discussed in Section V. The bold black line pictures the no-shock condition discussed in section IV. At $T < T_F$, no shock forms above this line, for the speed of sound becomes larger than the collision speed.

where N_1^* has been defined in Equation (12).

- In the intermediate regime when β_0 approaches unity, the value of the growth-rate has been interpolated (see Figure 6), $\delta = X\omega_{pp}$. One chooses $\max(b_C, b_Q) = b_Q$ since $\beta_r > \alpha$ to obtain

$$\frac{\nu_{ss}}{\delta} \sim \frac{\sqrt{\pi}}{X} \sqrt{\frac{n_0}{N_1^*}} R^{3/2} \frac{\beta_0}{(\beta_0^2 + 1) \beta_r^2 \gamma_r^2}. \quad (27)$$

- In the relativistic regime, Equation (21) with $\max(b_C, b_Q) = b_Q$, is to be compared with Equation (22). One obtains,

$$\frac{\nu_{ss}}{\delta} \sim \frac{\sqrt{\pi}}{16} \sqrt{\frac{n_0}{N_1^*}} R^{3/2} \frac{2(1 + \beta_0^2) \sqrt{\gamma_0}}{\beta_0^2 (2\gamma_0^2 - 1)^2}. \quad (28)$$

The frontier between the collisional and the collisionless domains for shock formation is displayed in Figure 7.

D. Conditions on n_0 and γ_0 for a collisionless downstream

The strongly coupled regime in the (T, n) parameter space is similar to the one shown in Figure 4. Replacing the electron mass by the proton mass in the calculations yields a threshold density for weakly coupled degenerate plasmas of

$$n > \frac{8}{9\pi^4} \frac{m_p^3 q^6}{\hbar^6} = 3.88 \times 10^{32} \text{ cm}^{-3}. \quad (29)$$

Note that for classical plasmas, the weakly coupled regime still demands $k_B T > q^2 n^{1/3}$.

The calculations conducted in Section A to determine $n(n_0, \gamma_0)$ and $T(n_0, \gamma_0)$ are straightforwardly adapted. Equation (A7) now read $k_B T = (1/2)m_p v_0^2$ and $n = (\hat{\gamma} + 1)/(\hat{\gamma} - 1)n_0$, where the 1/2 factor in the first equation accounts for the fact that the initial kinetic energy of the electrons is negligible compared to that of the protons ($k_B T \sim \frac{1}{2}m_p v_0^2$).

The downstream of the formed shock will therefore be collisional if

$$n_0 < 3.88 \times 10^{32} \frac{\hat{\gamma} - 1}{\hat{\gamma} + 1} \text{ cm}^{-3}, \quad (30)$$

when degenerate, and

$$n_0 > \frac{1}{8} \left(\frac{\hat{\gamma} - 1}{\hat{\gamma} + 1} \right) \left(\frac{m_p c^2}{q^2} \right)^3 \beta_0^6 = 3.47 \times 10^{46} \frac{\hat{\gamma} - 1}{\hat{\gamma} + 1} \beta_0^6, \quad (31)$$

when classical.

The corresponding region is pictured in Figure 8. The intersection of the two strongly coupled limits is found at the same initial velocity as for the pair plasma, since the relevant value of β_0 (Equation 19) does not depend on the mass.

IV. ABOUT THE SMALL VELOCITY SPREAD REGIME: THE “NO-SHOCK” CONDITION

In the calculations presented above, we neglected any velocity spread Δv within the shells, that is, we assumed $\Delta v \ll v_r$. Noteworthily, shock formation cannot occur at low collision velocity, i.e., in the regime $\Delta v > v_r$, since the speed of sound c_s is proportional to Δv (with a proportionality constant of order unity). The equality $\Delta v \propto c_s = v_r$ indicates therefore the limit beyond which no shock forms, which is also the limit of our calculations.

Cold plasmas having $T < T_F$ are degenerate (see Figure 4). In this regime, the speed of sound is a function of the Fermi temperature T_F , hence of the density. On the other hand,

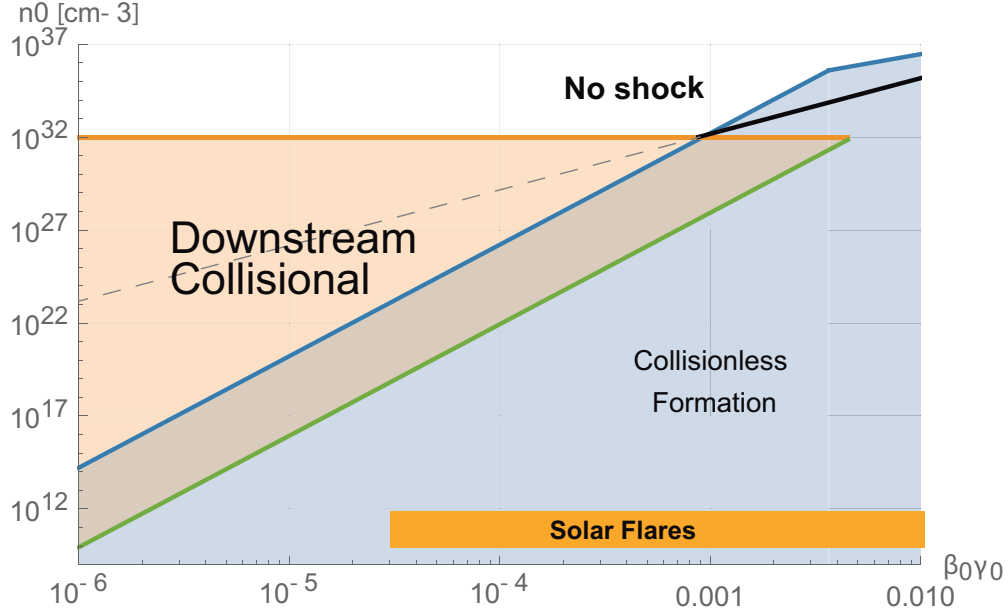


FIG. 8: If the electron/proton plasma shells have their initial $(\beta_0\gamma_0, n_0)$ located inside the pale orange triangle, the downstream is collisional and the resulting shock cannot accelerate particles. We considered $\hat{\gamma} = 5/3$. The colored region pertains to the solar flares scenario discussed in Section V. The bold black line pictures the no-shock condition discussed in section IV. At $T < T_F$, no shock forms above this line, for the speed of sound becomes larger than the collision speed.

for $T > T_F$ the colliding shells are classical and the speed of sound becomes a function of the temperature. Let us now assess the limit $c_s = v_r$ first for degenerate plasma, and then in the classical regime.

A. “No-shock” condition for cold, degenerate plasma

Since the Fermi temperature increases with the density, for a given shell encounter speed v_r the condition for shock formation, $v_r > c_s$ implies the existence of a critical (maximal) density, $n_{0,ns}$ [60] beyond which the encounter cannot produce a shock. At higher densities $n > n_{0,ns}$, the Fermi temperature T_F , hence the speed of sound, is larger than the relative speed of the collision.

In order to find the no-shock condition one needs to discriminate between the strongly coupled and the weakly coupled regimes. In the weakly coupled regime, simple analytical

expressions exist in the non-relativistic (Newtonian) and the ultra-relativistic limits.

1. *Weakly coupled plasma regime*

The general expressions for the energy density and the pressure in a degenerate Fermi gas is given by [29],

$$u = \frac{c}{8\pi^2\hbar^3} \left\{ p_F (2p_F^2 + m^2c^2) \sqrt{p_F^2 + m^2c^2} - (mc)^4 \sinh^{-1} \left(\frac{p_F}{mc} \right) \right\}, \quad (32)$$

$$P = \frac{c}{8\pi^2\hbar^3} \left\{ p_F \left(\frac{2}{3}p_F^2 - m^2c^2 \right) \sqrt{p_F^2 + m^2c^2} + (mc)^4 \sinh^{-1} \left(\frac{p_F}{mc} \right) \right\}, \quad (33)$$

where

$$p_F = (3\pi^2)^{1/3} n^{1/3} \hbar \quad (34)$$

is the Fermi momentum, and m is the particle mass (electron or proton).

Simple expressions which enable exact analytical calculations exist in both the Newtonian and the ultra-relativistic limits. In the Newtonian limit, $p_F \ll mc$, Equations (32, 33) are approximated by

$$u(N.R.) \simeq \frac{3(3\pi^2)^{2/3} \hbar^2}{10} n^{5/3}, \quad P(N.R.) = \frac{2}{3} u(N.R.). \quad (35)$$

On the other hand, in the ultra-relativistic limit, $p_F \gg mc$ one obtains [30],

$$u(rel.) \simeq \frac{3}{8} \left(\frac{3}{\pi} \right)^{1/3} hc n^{4/3}, \quad P(rel.) = \frac{u(rel.)}{3}. \quad (36)$$

The general expression for the speed of sound in a degenerate Fermi gas, which is correct in both the Newtonian and relativistic regimes is $c_s^2 = c^2 \frac{dP}{d\bar{u}}$, where $\bar{u} = nmc^2 + u$. In the Newtonian regime, $u \ll nmc^2$, this reduces to $c_s^2 = p_F^2/3m^2$, while in the ultra-relativistic regime $c_s^2 = c^2/3$, similar to the well-known result obtained for classical gas.

In order to find the criteria for shock formation, it is easier to work in the comoving frame of one of the colliding shells. The comoving density n is related to the lab-frame density n_0 by $n = n_0/\gamma_0$. In this frame the second shell is approaching at velocity v_r , given by Equation (2). Equating this velocity with the speed of sound, c_s , one finds the maximal density that allows formation of shock. In the Newtonian regime this density is

$$n_{0,ns} = \frac{8\sqrt{3}}{\pi^2} \left(\frac{mc}{\hbar} \right)^3 \frac{\beta_0^3}{(1 + \beta_0^2)^3} \gamma_0. \quad (37)$$

In the relativistic regime, equating the colliding speed v_r with the sound speed $c_s = c/\sqrt{3}$ results in an asymptotic value of β_0 ,

$$\beta_0 = \sqrt{3} - \sqrt{2} \sim 0.32 \quad \Rightarrow \quad \beta_0 \gamma_0 = \frac{1}{2} \sqrt{\sqrt{6} - 2} \sim 0.33. \quad (38)$$

We thus conclude that at faster shells velocities encounter, shock waves will always form.

2. Strongly coupled plasma regime

At sufficiently low temperatures and low densities, namely $n_0 < 6.3 \times 10^{22} \text{ cm}^{-3}$ (i.e. Fermi energy $E_F < q^2 n^{1/3}$) the plasma particles are strongly coupled. In this regime, the Fermi energy is lower than the Coulomb potential. To the best of our knowledge, there is no simple expression for the speed of sound in pair plasmas in this regime [61]. Study of the plasma in this regime is clearly outside the scope of the present work, and we therefore leave it for a future study. We therefore represent the no-shock boundary in this regime using dashed lines in Figures 3, 5, 7 and 8.

The no-shock criteria is plotted in thick black lines in Figures 3 and 5 for the pair plasmas scenario. No shocks can be formed above these lines. In the case of electron/proton plasma, these calculations can be straightforwardly adapted replacing the electron mass by the proton mass. The corresponding criteria is plotted by thick black lines in Figures 7 and 8.

B. “No-shock” condition in the classical plasma regime

As long as $T < T_F(n)$, the shells can be regarded as cold, and the degenerate results at $T=0$ apply. However, at sufficiently low densities, $T > T_F(n)$, the speed of sound varies with the temperature rather than the density.

In this classical regime, the speed of sound is given by $c_s = c\sqrt{(\partial P/\partial u)_s}$, where u is the energy density. Simple analytical expressions exist in the non-relativistic ($T \ll mc^2$) and relativistic ($T \gg mc^2$) limits:

$$c_s = \begin{cases} \sqrt{\hat{\gamma} \frac{k_B T}{m}} & (T \ll mc^2), \\ \frac{c}{\sqrt{3}} & (T \gg mc^2). \end{cases} \quad (39)$$

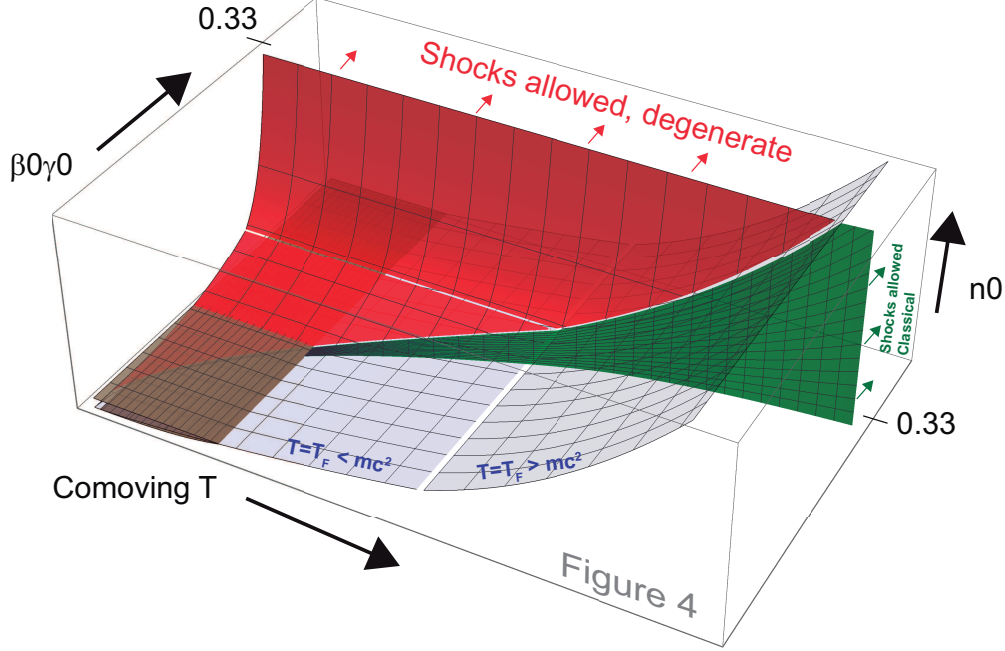


FIG. 9: Sketch (not to scale) of the various domains involved in the article, in the phase space of parameters (n_0, β_0, T) . Shock formation is only allowed for systems located behind the red surface, or behind the green surface. No shock is formed in the rest of the parameter space, because the speed of sound exceeds the speed of the collision. Figure 4 corresponds to a 2D cut at $\beta_0\gamma_0 = 0$, of this 3D plot.

Here, $\hat{\gamma}$ is the adiabatic index.

Similar to the degenerate case, in order for the shock to form, the requirement is $v_r > c_s$. Using Equation 2, one finds that for low, non-relativistic temperatures, the minimum velocity scales as $\beta_0 \propto \sqrt{T}$. For hot (relativistic) plasmas, the speed of sound is the same in both the classical and the degenerate regimes, and therefore the minimum value of β_0 that enables the production of shocks saturates to the value of β_0 given by Equation (38). This coincidence of the degenerate and classical values of the minimum of β_0 allowed for shock formation was to be expected, since both merge for $T = T_F$.

C. Complete parameter space region for shock formation

The results of this section are summarized in Figure 9. This figure generalizes the results presented in Figures 3, 5, 7 and 8 by adding a third dimension, namely, the co-moving shells

temperature.

The purple surface pictures systems with $T = T_F$. Above it, the plasma is degenerate, while below it is classical. As is evident, the slope breaks at $k_B T = mc^2$, as at lower temperatures the plasma is non-relativistic and $T_F \propto n^{2/3}$, while in the relativistic limit $T_F \propto n^{1/3} \rightarrow n \propto T_F^3$. This purple surface divides the parameter space into two regimes: above this surface, $T < T_F$ and the plasma is degenerate, while below this surface, $T > T_F$ and the plasma is classical.

The two brown surfaces represent the $k_B T = q^2 n_0^{1/3}$ and $k_B T_F = q^2 n_0^{1/3}$ limits. Systems located between these two surfaces are strongly coupled. These surfaces therefore represent a 3-dimensional extension of the results presented in Figure 4 (red lines).

The red/green surfaces picture the “no shock” condition ($v_r < c_s$) in the degenerate/classical plasmas, respectively. In both regimes, as long as the plasma is in the Newtonian regime, increasing the temperature requires an increase in the collision velocity β_0 as $\beta_0 \propto T^{1/2}$ in order to enable the formation of shock. Thus, shocks can only be formed “outside” of the pictured surfaces.

As the density increases, the Fermi temperature becomes relativistic, $T_F > mc^2$, and the condition on the collision velocity saturates, to $\gamma_0 \beta_0 \simeq 0.33$ (see Equation 38). At higher collision speeds, shock could always form, regardless of the initial densities, the plasma temperatures or the nature of the plasma, being either classical or degenerate.

V. ASTROPHYSICAL IMPLICATIONS

A key difference between collisional and collisionless shocks rely on the (theoretical) ability of the later to both accelerate particles to high energies as well as generate strong magnetic fields. These phenomena cannot occur in collisional shocks, due to the rapid thermalization of the plasma in the downstream region, which suppresses the growth of any seed magnetic fields, as well as thermalize energetic particles [e.g. 16].

Relativistic outflows in the form of astronomical jets are most easily observed at the exterior of many astronomical objects, ranging from supernova, X-ray emitting binaries (neutron stars or black holes) [31, 32], gamma-ray bursts (GRBs) [33, 34] or supermassive black holes in active galactic nuclei (AGNs) [35, 36]. While these objects inevitably involve shock waves, the low environmental densities imply that these shocks are formed collisionless,

and so are their downstream regions.

The situation is somewhat more complicated in the interior of the various astronomical objects. We plot in Figure 7 typical values of the interior density as well as the normalized velocities associated with random fluctuations of different objects. The velocities are derived based on temperature estimate in the interior of the different objects, considering that forming a shock requires motions faster than the thermal velocity. We consider the solar interior, cooled white dwarfs (WD) (whose temperature vary in the range $3 \times 10^5 - 10^9$ °K) [37], and neutron stars (NS), having characteristic temperatures of 0.1 – 30 MeV [38]. While shock waves that are generated in the interior of main sequence stars and WDs are always in the collisionless regime, shocks that can potentially form in the interior of NS can in principle be generated in the collisional regime, though they may fall into the “no shock” parameter space region. As these shocks propagate outwards, they will eventually propagate towards lower density and potentially higher velocities regime, and may therefore move into the collisionless regime of the parameter space.

Pair dominated plasmas are expected to occur in few astronomical scenarios. One of the widely discussed scenarios is that of pair-instability supernovae. Massive stars ($M \gtrsim 100M_\odot$) form large helium cores that reach carbon ignition with masses in excess of $\sim 45M_\odot$. After helium burning, cores of this mass will encounter the electron-positron pair instability, collapse and ignite oxygen and silicon burning explosively. If explosive oxygen burning provides enough energy, the result is a “pair-instability supernovae” [39, 40]. In recent years, there were several observational evidence for this mechanism, e.g., in SN2006gy [41] or SN2007bi [42]. In Figure 3, we plot possible parameter space values for this scenario.

A second scenario is that of gamma-ray bursts (GRBs). The leading model to explain the observed variable light-curves in these objects, the GRB “fireball” model [43] invokes internal shocks. These shocks can in principle occur at radii as small as a few times the Schwarzschild radius of $\sim 10 M_\odot$ black hole, namely at $\gtrsim 10^7$ cm. The densities are similar to that at the interior of massive stars. As these shocks occur below the photosphere, a significant number of pairs are created [44]. Equilibration between pair production and annihilation results in density ratio of $n_\pm/n_e \sim 10$ [45]. The typical values of density and velocity in this scenario is similar to that of pair-instability supernovae, and is similarly plotted in Figure 3.

We thus conclude that in these objects, the shock waves can initially be formed as colli-

sional, though as they propagate outward, they become collisionless. As a consequence, the time available for particle acceleration and magnetic field generation in these shock waves could be limited.

Another environment of interest is that of solar flares. With typical electron densities of $\sim 10^{10} - 10^{12} \text{ cm}^{-3}$ [46] and typical velocities in the range $30 - 10^4 \text{ km/s}$ [46, 47], the resulting shock waves are expected to be formed collisionless, but the downstream region of the low velocity shocks (at least, initially) could potentially be collisional. While the flares will eventually propagate into lower density region, these conditions limit their ability to accelerate particles at their initial phases. The corresponding parameter space values are plotted on Figure 8.

VI. CONCLUSIONS

This article deals with the properties of the shock waves that are formed when two symmetrical plasmas run into each other, and in particular in the question of collisionality. We assessed the answers to two questions: 1/ When is the interaction mediated by close Coulomb binary collisions or collective plasma instabilities? and 2/ Once a shock has been formed, when is its downstream collisionless?

The answer to the first question is given in Figure 3 for the pair plasmas and Figure 7 for the electron-proton plasmas. The answer to the second question is presented in Figures 5 & 8 for pair and electron-proton plasmas respectively.

As we showed here, the switch from collisional to collisionless regime bears consequences on the time scale of the shock formation. In the collisionless regime, the shock formation time is determined by the growth-rate of the unstable interaction between the two shells. In the collisional regime, on the other hand, the shock formation time is set by the frequency of close binary collisions.

Moreover, a shock whose formation not mediated by collisionless plasma instabilities will not inherit the downstream electromagnetic patterns formed by these instabilities. Collisions of shells with curved boundaries may trigger downstream vorticity that could generate magnetic fields [48]. But colliding planar shells like those considered here, will yield a field-free downstream if the formation is collisional.

Understanding the properties of the downstream region (the second question outlined

above) has the important consequence of determining the ability of the downstream region to accelerate particles. As discussed above, a collisional downstream leads to a suppression of particle acceleration. For two plasma shells initially located in the orange triangle plotted in Figure 5 for pair plasmas, or Figure 8 for electron/proton plasmas, the resulting shock will not be able to accelerate particles. As a result, the radiative signature of the system would be dramatically different than that of a system in which the downstream is collisionless.

In Section V, we discussed several astrophysical settings where a shock may be formed as collisional, and, during its propagation inside the object, its properties will be modified from a collisional to a collisionless medium. The key consequences of this transition is the limiting ability of these shocks to accelerate particles to high energies and to generate magnetic fields. This implies stringent constraints on the abilities of these objects to be the sources of high energy cosmic rays, as well as modification of the resulting spectra. We leave a detailed study of the spectra expected under various conditions to future work. Similar situations can be found in the context of Inertial Confinement Fusion [49]. While the medium considered here are spatially homogeneous, it would be worth studying how a shock transiting from one kind of medium to another, evolves.

In this work, we focused on “classical” shocks, namely shocks that are mediated either by collective plasma effects or by Coulomb collisions. If shock waves occur in regions of high optical depth in which the mean free path is smaller than the shock size, they may be mediated by photons scattered back and forth the upstream and downstream regions [44, 50, 51]. This scenario is further expected to modify the shock properties; in particular, no particle acceleration is expected. We leave a full treatment of the properties of these radiative-mediated shocks to a future work.

Encounter of partially ionized shells could be worthy of investigation. In such a setting, the outcome may sharply depend on the intra-shell coupling between the ionized and the neutral particles. If intra shells collisions are rare, both component may act separately. The ionized part should form a collisionless shock on a time scale given by plasma instabilities. Meanwhile, the neutral component could form a shock on a time scale defined by the collision frequency between neutrals of different shells. But if both components are coupled, then the first one to form a shock may drag the other into the formation of a single, common, shock. Such scenarios will be studied in future works.

Future works could also focus on studying temperature effects. The present calculations

are valid as long as the shells' velocity spread Δv fulfills $\Delta v \ll v_r$. Larger spreads should affect the binary collisions frequencies, the maximum growth-rates, and also the Rankine-Hugoniot (RH) conditions used to determine the collisionality of the downstream. While such effects on the binary collisions frequencies, or on the RH conditions are accessible, there are so far no analytical formulas available for the maximum growth-rate in terms of the temperature and γ_0 [52]. Such progresses are therefore a prerequisite before one can elaborate on larger temperature effects. Note however that as discussed in section IV, no shock should form when $\Delta v > v_r$ since the speed of sound becomes larger than the collision speed in this limit. Therefore, as far as the velocity spread is concerned, this work investigates the case $\Delta v/v_r \ll 1$, and the regime left to explore is simply $\Delta v/v_r$ of order unity.

VII. ACKNOWLEDGMENTS

A.B. acknowledges support by grant ENE2016-75703-R from the Spanish Ministerio de Educación. A.P. acknowledges support by the European Union Seventh Framework Program (FP7/2007-2013) under grant agreement no. 618499, and support from NASA under grant no. NNX12AO83G. A.B. thanks Gustavo Wouchuk and Roberto Piriz for fruitful discussions.

Appendix A: Determination of $n(n_0, \gamma_0)$ and $T(n_0, \gamma_0)$

The fact that the collisional regime lies deep within the non-relativistic domain as is shown in Figure 4, suggests that a non-relativistic treatment is appropriate. Once the shock is formed, the shock frame is well defined. In this frame, we use the subscripts “1” (“2”) to describe upstream (downstream) quantities. In the non-relativistic regime and for zero upstream pressure ($P_1 = 0$), the Rankine-Hugoniot (RH) relations read [5],

$$\begin{aligned} \frac{n_2}{n_1} &= \frac{\rho_2}{\rho_1} = \frac{\hat{\gamma} + 1}{\hat{\gamma} - 1}, \\ \frac{v_2}{v_1} &= \frac{\hat{\gamma} - 1}{\hat{\gamma} + 1}. \end{aligned} \tag{A1}$$

Here, $\hat{\gamma}$ is the adiabatic index of the gas, the ρ_1, ρ_2, v_1, v_2 are the mass densities, upstream and downstream velocities respectively. The RH relation for the downstream pressure P_2

leads to

$$\begin{aligned}
P_2 &= \rho_1 v_1^2 - \rho_2 v_2^2 \\
&= \rho_1 v_1^2 - \rho_1 \frac{\hat{\gamma} + 1}{\hat{\gamma} - 1} \left(v_1 \frac{\hat{\gamma} - 1}{\hat{\gamma} + 1} \right)^2 \\
&= \rho_1 v_1^2 \frac{2}{\hat{\gamma} + 1}.
\end{aligned} \tag{A2}$$

Since the plasma is non relativistic, the upstream velocity as written in the downstream frame is simply $\beta_0 = v_0/c$. One thus have,

$$v_0 = v_1 - v_2 = v_1 - \frac{\hat{\gamma} - 1}{\hat{\gamma} + 1} v_1 = \frac{2}{\hat{\gamma} + 1} v_1. \tag{A3}$$

Using this result in Equation (A2) then gives,

$$\begin{aligned}
P_2 &= \rho_1 v_1^2 \frac{2}{\hat{\gamma} + 1} = \rho_1 \left(\frac{\hat{\gamma} + 1}{2} v_0 \right)^2 \frac{2}{\hat{\gamma} + 1} \\
&= \rho_0 \frac{\hat{\gamma} + 1}{2} v_0^2 = 2n_0 m_e \frac{\hat{\gamma} + 1}{2} v_0^2,
\end{aligned} \tag{A4}$$

where ρ_1 has been replaced by ρ_0 in the last line, as no relativistic boosting exists, while the factor 2 comes because there are n_0 electrons and n_0 positrons per unit volume.

Denoting the energy density by u , the downstream pressure P_2 reads,

$$P_2 = (\hat{\gamma} - 1)\rho u = (\hat{\gamma} - 1)nk_B T. \tag{A5}$$

One finally obtains,

$$nk_B T = m_e \frac{\hat{\gamma} + 1}{\hat{\gamma} - 1} n_0 v_0^2, \tag{A6}$$

namely

$$\begin{aligned}
k_B T &= m_e v_0^2, \\
n &= n_0 \frac{\hat{\gamma} + 1}{\hat{\gamma} - 1},
\end{aligned} \tag{A7}$$

which are the relations we needed. The first one reads $k_B T = \frac{1}{2} (2m_e v_0^2)$, which simply states that the downstream thermal energy originates from the upstream kinetic energy.

Appendix B: Derivation of the dispersion equation (23)

Suppose we have $a \in \mathbb{N}$ cold beams made of species of densities n_j , masses m_j and velocities $\mathbf{v}_j = v_j \mathbf{e}_z$, the system being overall charge and current neutral. The dispersion

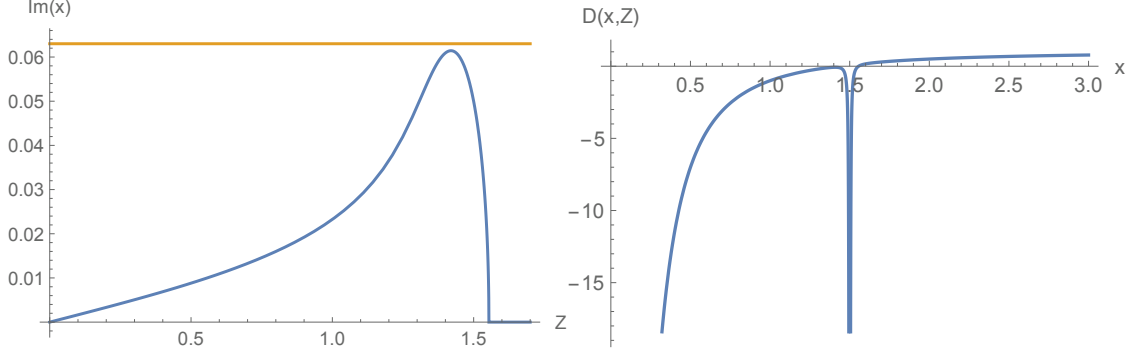


FIG. 10: **LEFT**: growth-rate given by $\text{Im}(x)$ with $x/D(x, Z) = 0$ for $R = 1/1836$. The orange line shows the result given by Equation (24). **RIGHT**: Plot of the dispersion function $D(x, Z)$ defined in Equation (B2), for $R = 1/1836$ and $Z = 1.5$.

equation for longitudinal waves with $\mathbf{k} \parallel \mathbf{e}_z$ reads (see [53], p. 137),

$$\sum_{j=1}^a \frac{\omega_{pj}^2}{(\omega - \mathbf{k} \cdot \mathbf{v}_j)^2} = 1, \quad (\text{B1})$$

where $\omega_{pj}^2 = 4\pi n_j q^2 / m_j$ is the plasma frequency of specie j . The unstable system considered in Section III B accounts for 3 species: the 2 counter-streaming proton beams, and the cold electronic background. With the dimensionless variables used, (B1) then gives,

$$D(x, Z) \equiv \frac{2}{x^2} + \frac{R}{(Z - x)^2} + \frac{R}{(x + Z)^2} - 1 = 0, \quad (\text{B2})$$

which is Equation (23).

This dispersion equation can be derived either using a multiple cold fluids model [54], or taking the kinetic dispersion equation for such waves, and considering a distribution function which is the sum of Dirac delta functions (like in [53]).

The growth-rate $\text{Im}(x)$, with $x/D(x, Z) = 0$, is plotted on Figure 10-Left for $R = 1/1836$. It reaches a maximum near $Z = \sqrt{2}$. This can be understood noting that since $R \ll 1$, the roots of the equation have to be close to the roots of the same equation, but with $R = 0$, that is $x = \pm\sqrt{2}$. It follows that for $0 < R \ll 1$, the numerators of the terms $\propto R$ have to be small if these terms are to bring a significant contribution to the equation. This implies in turn $Z \sim \pm\sqrt{2}$.

The dispersion function $D(x, Z)$ is plotted on Figure 10-Right for $x > 0$, $R = 1/1836$ and $Z = 1.5$. It is an even function of x , which is the reason why only the $x > 0$ part is plotted.

Let us now focus on the root located near $x = \sqrt{2}$. It is primarily determined by the terms $2/x^2$ and $R/(x - Z)^2$ of the dispersion equation. We can therefore study the solution located near $x = \sqrt{2}$ by neglecting $R/(x + Z)^2$, that is, solving,

$$\frac{2}{x^2} + \frac{R}{(Z - x)^2} = 1. \quad (\text{B3})$$

We can solve approximately this equation following a method derived long ago [55]. Knowing that the maximum growth-rate δ is found for $x \sim \sqrt{2}$, we write $x = \sqrt{2} + i\delta$, with $\delta \in \mathbb{R}$. We then assume $|Z - \sqrt{2}| \ll |\delta|$ (which is later verified) so that Equation (B3) becomes,

$$\frac{2}{(\sqrt{2} + i\delta)^2} - \frac{R}{\delta^2} = 1. \quad (\text{B4})$$

A Taylor expansion of the first term, and some straightforward algebra, gives the growth-rate (24).

-
- [1] A. R. Bell. The acceleration of cosmic rays in shock fronts. I. *Mon. Not. R. Astron. Soc.*, 182:147–156, January 1978.
 - [2] L. O. Silva, R. A. Fonseca, J. W. Tonge, J. M. Dawson, W. B. Mori, and M. V. Medvedev. Interpenetrating Plasma Shells: Near-equipartition Magnetic Field Generation and Nonthermal Particle Acceleration. *Astrophys. J.*, 596:L121–L124, October 2003.
 - [3] A. Spitkovsky. Particle Acceleration in Relativistic Collisionless Shocks: Fermi Process at Last? *Astrophys. J.*, 682:L5–L8, July 2008.
 - [4] L. Sironi and A. Spitkovsky. Particle Acceleration in Relativistic Magnetized Collisionless Electron-Ion Shocks. *Astrophys. J.*, 726:75–+, January 2011.
 - [5] Ya B Zel'dovich and Yu P Raizer. *Physics of shock waves and high-temperature hydrodynamic phenomena*. Dover Publications, 2002.
 - [6] H. E. Petschek. Aerodynamic Dissipation. *Reviews of Modern Physics*, 30:966–974, July 1958.
 - [7] R. Z. Sagdeev. Cooperative Phenomena and Shock Waves in Collisionless Plasmas. *Reviews of Plasma Physics*, 4:23, 1966.
 - [8] A. Bamba, R. Yamazaki, M. Ueno, and K. Koyama. Small-Scale Structure of the SN 1006 Shock with Chandra Observations. *Astrophys. J.*, 589:827–837, June 2003.
 - [9] Roald Z Sagdeev and Charles F Kennel. Collisionless shock waves. *Scientific American*, 264(4):106–115, 1991.

- [10] S. D. Bale, F. S. Mozer, and T. S. Horbury. Density-transition scale at quasiperpendicular collisionless shocks. *Phys. Rev. Lett.*, 91:265004, Dec 2003.
- [11] Steven J. Schwartz, Edmund Henley, Jeremy Mitchell, and Vladimir Krasnoselskikh. Electron temperature gradient scale at collisionless shocks. *Phys. Rev. Lett.*, 107:215002, Nov 2011.
- [12] A. Bret, A. Stockem, F. Fiúza, C. Ruyer, L. Gremillet, R. Narayan, and L. O. Silva. Collisionless shock formation, spontaneous electromagnetic fluctuations, and streaming instabilities. *Physics of Plasmas*, 20:042102, 2013.
- [13] A. Bret, A. Stockem, R. Narayan, and L. O. Silva. Collisionless weibel shocks: Full formation mechanism and timing. *Physics of Plasmas*, 21(7):072301, 2014.
- [14] R Blandford and D Eichler. Particle acceleration at astrophysical shocks: A theory of cosmic ray origin. *Phys. Rep.*, 154:1, 1987.
- [15] A Marcowith, A Bret, A Bykov, M E Dieckmann, L OC Drury, B Lembège, M Lemoine, G Morlino, G Murphy, G Pelletier, I Plotnikov, B Reville, M Riquelme, L Sironi, and A Stockem Novo. The microphysics of collisionless shock waves. *Reports on Progress in Physics*, 79:046901, 2016.
- [16] M. S. Longair. *High Energy Astrophysics*. February 2011.
- [17] M. Milosavljevic and Nakar. Weibel filament decay and thermalization in collisionless shocks and gamma-ray burst afterglows. *Astrophys. J.*, 641:978–983, 2006.
- [18] C. M. Huntington, F. Fiuza, J. S. Ross, A. B. Zylstra, R. P. Drake, D. H. Froula, G. Gregori, N. L. Kugland, C. C. Kuranz, M. C. Levy, C. K. Li, J. Meinecke, T. Morita, R. Petrasso, C. Plechaty, B. A. Remington, D. D. Ryutov, Y. Sakawa, A. Spitkovsky, H. Takabe, and H.-S. Park. Observation of magnetic field generation via the Weibel instability in interpenetrating plasma flows. *Nature Physics*, 11:173–176, February 2015.
- [19] Anatoly Spitkovsky. Particle acceleration in relativistic collisionless shocks: Fermi process at last? *Astrophys. J. Lett.*, 682:L5–L8, 2008.
- [20] J.D. Jackson. *Classical Electrodynamics*. Wiley, 1998.
- [21] G.B. Rybicki and A.P. Lightman. *Radiative Processes in Astrophysics*. John Wiley & Sons, 1979.
- [22] K. M. Watson, S. A. Bludman, and M. N. Rosenbluth. Statistical mechanics of relativistic streams. i. *Phys. Fluids*, 3:741, 1960.
- [23] A. Bret, L. Gremillet, and M. E. Dieckmann. Multidimensional electron beam-plasma insta-

- bilities in the relativistic regime. *Phys. Plasmas*, 17:120501, 2010.
- [24] MV Medvedev, M Fiore, RA Fonseca, LO Silva, and WB Mori. *Astrophys. J.*, 618:L75, 2005.
- [25] N.W. Ashcroft and N.D. Mermin. *Solid State Physics*. HRW international editions. Holt, Rinehart and Winston, 1976.
- [26] Setsuo Ichimaru. Strongly coupled plasmas: high-density classical plasmas and degenerate electron liquids. *Rev. Mod. Phys.*, 54:1017–1059, Oct 1982.
- [27] A. Stockem Novo, A. Bret, R. A. Fonseca, and L. O. Silva. Shock formation in electron-ion plasmas: Mechanism and timing. *The Astrophysical Journal Letters*, 803(2):L29, 2015.
- [28] R. Shaisultanov, Y. Lyubarsky, and D. Eichler. Stream instabilities in relativistically hot plasma. *The Astrophysical Journal*, 744:182, 2012.
- [29] L.D. Landau and E.M. Lifshitz. *Course of Theoretical Physics, Statistical Physics*. Number v. 5. Elsevier Science, 2013.
- [30] S. Chandrasekhar. The Maximum Mass of Ideal White Dwarfs. *Astrophysical Journal*, 74:81, July 1931.
- [31] R. Fender. *Jets from X-ray binaries*. April 2006.
- [32] R. Fender. Disc-jet-wind coupling in black hole binaries, and other stories. *Astronomische Nachrichten*, 337:381, May 2016.
- [33] P. Mészáros. Gamma-ray bursts. *Reports on Progress in Physics*, 69:2259–2321, August 2006.
- [34] A. Pe’er. Physics of Gamma-Ray Bursts Prompt Emission. *Advances in Astronomy*, 2015:907321, 2015.
- [35] M. C. Begelman, R. D. Blandford, and M. J. Rees. Theory of extragalactic radio sources. *Reviews of Modern Physics*, 56:255–351, April 1984.
- [36] C. M. Urry and P. Padovani. Unified Schemes for Radio-Loud Active Galactic Nuclei. *Publ. Astr. Soc. Pacific*, 107:803–845, September 1995.
- [37] S. L. Shapiro and S. A. Teukolsky. *Black holes, white dwarfs, and neutron stars: The physics of compact objects*. 1983.
- [38] J. M. Lattimer and M. Prakash. Neutron star observations: Prognosis for equation of state constraints. *Phys. Rep.*, 442:109–165, April 2007.
- [39] J. R. Bond, W. D. Arnett, and B. J. Carr. The evolution and fate of Very Massive Objects. *Astrophys. J.*, 280:825–847, May 1984.
- [40] A. Heger and S. E. Woosley. The Nucleosynthetic Signature of Population III. *Astrophys. J.*

- , 567:532–543, March 2002.
- [41] N. Smith, W. Li, R. J. Foley, J. C. Wheeler, D. Pooley, R. Chornock, A. V. Filippenko, J. M. Silverman, R. Quimby, J. S. Bloom, and C. Hansen. SN 2006gy: Discovery of the Most Luminous Supernova Ever Recorded, Powered by the Death of an Extremely Massive Star like η Carinae. *Astrophys. J.* , 666:1116–1128, September 2007.
- [42] A. Gal-Yam, P. Mazzali, E. O. Ofek, P. E. Nugent, S. R. Kulkarni, M. M. Kasliwal, R. M. Quimby, A. V. Filippenko, S. B. Cenko, R. Chornock, R. Waldman, D. Kasen, M. Sullivan, E. C. Beshore, A. J. Drake, R. C. Thomas, J. S. Bloom, D. Poznanski, A. A. Miller, R. J. Foley, J. M. Silverman, I. Arcavi, R. S. Ellis, and J. Deng. Supernova 2007bi as a pair-instability explosion. *Nature (London)* , 462:624–627, December 2009.
- [43] M. J. Rees and P. Meszaros. Unsteady outflow models for cosmological gamma-ray bursts. *Astrophys. J.*, 430:L93–L96, August 1994.
- [44] A. M. Beloborodov. Sub-photospheric Shocks in Relativistic Explosions. *Astrophys. J.* , 838:125, April 2017.
- [45] A. Pe’er and E. Waxman. Prompt Gamma-Ray Burst Spectra: Detailed Calculations and the Effect of Pair Production. *Astrophys. J.* , 613:448–459, September 2004.
- [46] M. J. Aschwanden. Particle acceleration and kinematics in solar flares - A Synthesis of Recent Observations and Theoretical Concepts (Invited Review). *Space Science Rev.*, 101:1–227, January 2002.
- [47] N. L. S. Jeffrey, L. Fletcher, and N. Labrosse. Non-Gaussian Velocity Distributions in Solar Flares from Extreme Ultraviolet Lines: A Possible Diagnostic of Ion Acceleration. *Astrophys. J.* , 836:35, February 2017.
- [48] D. Bond, V. Wheatley, R. Samtaney, and D. I. Pullin. Richtmyer-meshkov instability of a thermal interface in a two-fluid plasma. *Journal of Fluid Mechanics*, 833:332363, 2017.
- [49] Wen-Shuai Zhang, Hong-Bo Cai, Lian-Qiang Shan, Hua-Sen Zhang, Yu-Qiu Gu, and Shao-Ping Zhu. Anomalous neutron yield in indirect-drive inertial-confinement-fusion due to the formation of collisionless shocks in the corona. *Nuclear Fusion*, 57(6):066012, 2017.
- [50] R. Budnik, B. Katz, A. Sagiv, and E. Waxman. Relativistic Radiation Mediated Shocks. *Astrophys. J.* , 725:63–90, December 2010.
- [51] C. Lundman, A. Beloborodov, and I. Vurm. Radiation mediated shocks in gamma-ray bursts: Pair creation. *ArXiv e-prints*, August 2017.

- [52] A. Bret, L. Gremillet, and D. Bénisti. Exact relativistic kinetic theory of the full unstable spectrum of an electron-beam plasma system with maxwell-jüttner distribution functions. *Phys. Rev. E.*, 81:036402, 2010.
- [53] S. Ichimaru. *Basic Principles of Plasma Physics*. W. A. Benjamin, Inc., Reading, Massachusetts, 1973.
- [54] F. Califano, R. Prandi, F. Pegoraro, and S. V. Bulanov. Nonlinear filamentation instability driven by an inhomogeneous current in a collisionless plasma. *Phys. Rev. E*, 58:7837, 1998.
- [55] S. A. Bludman, K. M. Watson, and M. N. Rosenbluth. Statistical mechanics of relativistic streams. ii. *Phys. Fluids*, 3:747, 1960.
- [56] E. Wigner. On the interaction of electrons in metals. *Phys. Rev.*, 46:1002–1011, Dec 1934.
- [57] D. Pines and P. Nozières. *The Theory of Quantum Liquids: Normal Fermi liquids*. The Theory of Quantum Liquids. W.A. Benjamin, 1966.
- [58] We focus the discussion here on shocks that propagate in an environment in which the energy density of radiation downstream can be neglected with respect to the particle thermal energy.
- [59] Note that in calculating the Coulomb potential there is a pre-factor of order unity, which is omitted for clarification.
- [60] The subscript “ns” in $n_{0,ns}$ stands for “no shock”.
- [61] For example, strongly coupled electrons over a neutralizing background can form a so-called “Wigner crystal” at high density [56, 57].